1.9 THz quantum-cascade lasers with one-well injector

Sushil Kumar, Benjamin S. Williams, and Qing Hu
Department of Electrical Engineering and Computer Science and Research Laboratory of Electronics, Massachusetts Institute of Technology, Cambridge, Massachusetts 02139

John L. Reno
Sandia National Laboratories, Department 1123, MS 0601, Albuquerque, New Mexico 87185-0601

(Received 12 December 2005; accepted 12 February 2006; published online 24 March 2006)

We report terahertz quantum-cascade lasers operating predominantly at 1.90 THz with side modes as low as 1.86 THz ($\lambda \approx 161$ μm, $\hbar\omega \approx 7.7$ meV). This is the longest wavelength to date of any solid-state laser that operates without assistance of a magnetic field. Carriers are injected into the upper radiative state by using a single quantum-well injector, which resulted in a significant reduction of free-carrier losses. The laser operated up to a heat-sink temperature of 110 K in pulsed mode, 95 K in continuous wave (cw) mode, and the threshold current density at 5 K was $\sim$140 A/cm^2. © *2006 American Institute of Physics*. [DOI: 10.1063/1.2189671]

Because of its very nature, the energy levels of the active region of a quantum-cascade laser (QCL) are aligned in such a way that it will result in a negative differential resistance (NDR) if it were an isolated structure. That is, when electrons traverse through the active region, their initial state is higher in energy than the final state. The same applies to the yet-to-be-developed Bloch oscillators. In order to avoid the current instability associated with such an energy-level alignment, the Bell Labs group developed an injector region based on a miniband formed by a graded superlattice structure,[1] which limits the current flow until the bias voltage corresponding to the desired energy alignment is applied. This scheme has paved the way for the successful development of mid-infrared quantum-cascade lasers (QCLs).[2] It has also worked well for terahertz (THz) QCLs below the *Reststrahlen* band in the chirped superlattice[3] and bound-to-continuum[4] schemes. However, as one pursues even lower-frequency QCLs below 2 THz that approaches the frequency range of electronic devices, this paradigm faces at least two major challenges. First, the intersubband energy separation below 2 THz ($\hbar\omega \sim 8$ meV) is so narrow that the injection selectivity of a miniband injector suffers when the miniband width is much greater than $\hbar\omega$. Second, and perhaps more important, the intersubband energy separation within the injector minibands now becomes comparable to $\hbar\omega$, thus absorption due to electrons residing at lower levels in the injector miniband becomes significant to prevent devices from reaching the lasing threshold. Previously, terahertz QCLs with two (or more) well injectors operating down to 2 THz ($\lambda \approx 150$ μm) have been demonstrated.[5,6] In this letter, we report the development of QCLs based on injectors with only one well. By careful design of the subbands in the active region, we have avoided the occurrence of a NDR before the design bias and have achieved lasing at 1.86 THz ($\lambda \approx 161$ μm) without the assistance of magnetic fields.

The intersubband dipole selection rule in QCLs precludes the electric field from coupling directly to the in-plane electron motion. Since most of the carriers reside in the injector region, the lack of additional subbands in a one-well injector will prevent reabsorption of terahertz radiation due to intersubband transitions, a mechanism that is a potential source of significant waveguide loss in multiple-well injectors. This is in contrast to very low frequency QCLs that have been demonstrated using strong magnetic fields applied perpendicular to the layers to increase modal gain by increasing lifetime of the upper radiative state and to decrease free carrier absorption in the structure by in-plane localization of carriers and subsequent quenching of intersubband scattering channels.[7] Figure 1(a) shows the conduction band diagram at a design bias of 46.5 mV/module for the present design. The four quantum well module grown in GaAs/Al$_{0.15}$Ga$_{0.85}$As is repeated multiple times to allow electron transport in a cascade scheme. At low electron temperatures, only four levels (1–4) in each module participate in the transport process. At resonance, electrons are injected into the upper level 4 via sequential tunneling from the injector level 1′ of the preceding module. After undergoing radiative and nonradiative transitions between levels 4 and 3, the electrons are extracted from lower level 3, which is in resonance with level 2. This is the so called resonant LO phonon scheme[8,9] which is a

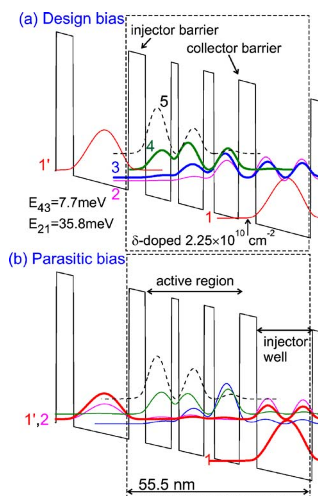

FIG. 1. (Color online) Calculated conduction band diagrams at the design bias (8.4 kV/cm, 46.5 mV/module) and the parasitic bias (6.65 kV/cm, 37 mV/module) with the four-well modules outlined in boxes. Starting from the injector barrier on the left, the layer thicknesses in Å are **49**/78/**23**/76/**32**/76/**52**/168 with barriers indicated by bold fonts, and the 52 Å collector barrier is delta-doped at 2.25×10^{10} cm^{-2} in the center.

0003-6951/2006/88(12)/121123/3/$23.00

© 2006 American Institute of Physics
Downloaded 24 Mar 2006 to 18.62.10.37. Redistribution subject to AIP license or copyright, see http://apl.aip.org/apl/copyright.jsp

combination of resonant tunneling through the collector barrier and fast longitudinal-optical (LO) phonon scattering into level 1, from where they are reinjected into the next module. The calculated injection anticrossing energy gap between levels 1′ and 4 is small (~1.0 meV), which, because of strong dephasing due to various scattering mechanisms, makes transport through the injector barrier incoherent.[10,11] Within a tight-binding framework, overdamped oscillations of the electron wave packet across the injector barrier, and not the upper level lifetime τ_4, are expected to be the bottleneck to current flow. The electron population thus remains mostly localized in the injector well.

A major goal of terahertz QCL design is to minimize injection of carriers into lower energy subbands at fields applied below the design bias. Such parasitic current channels can undesirably boost the threshold current density. In severe cases, when the current channel at the parasitic bias is stronger than at the design bias, an early NDR is developed causing current instability in the circuit and preventing the device from reaching the design bias.[11] For this design, the dominant parasitic bias condition of 37 mV/module is shown in Fig. 1(b), where level 1′ is in resonance with level 2 of the injector well in the next module. Such an alignment constitutes a strong parasitic current channel due to very fast LO phonon scattering from level 2 to 1 ($E_{21} \approx \hbar\omega_{\mathrm{LO}}$, $\tau_2 \lesssim 0.2$ ps for all bias values). For two (or more) well injectors, coupling between levels 1′ and 2 is minimized by preventing the injector states from aligning to form a doublet (or a miniband) until beyond the parasitic bias. But for such an injection mechanism to work, the barriers in the multiple well injector should not be too thick to allow the injector subbands to align correctly, and to keep them sufficiently conducting at the design bias. This favors the use of large miniband width, a strategy that faces the two challenges discussed in the leading paragraph, when it is greater than the photon energy. For this reason we have used a one-well injector that could maintain a better injection selectivity at lower frequencies. It may be noted that injectorless QCLs have been demonstrated in the mid-infrared[12,13] but those cannot be discussed in the context of terahertz QCLs since the design bias is much greater than the parasitic bias for such designs due to much larger radiative energies involved, making the low bias parasitic current channels relatively insignificant.

A one-well injector carries the risk of a strong parasitic coupling since the injector is conducting for all applied fields. In the present design, several steps were taken to minimize the aforementioned parasitic current channel due to the $1' \rightarrow 2$ alignment. First, thicker injector and collector barriers were used to decrease the parasitic coupling (calculated anticrossing gap between levels 1′ and $2 \approx 0.31$ meV). However this comes at the cost of some aspects of laser performance. A thicker collector barrier (52 Å) decreases the coherence of transport across the collector-barrier and slows depopulation[11] [calculated collector anticrossing gap between levels 3 and 2 was 2.8 meV for this design as compared to 4.0 meV in a two-well injector QCL operating at 3 THz (Ref. 14)]. A thicker injector barrier reduces the peak current density that determines the maximum operating temperature and peak output power of the laser. Second, the radiative transition was made spatially diagonal to reduce parasitic coupling, although this caused a reduction in the oscillator strength (calculated $f_{43} \approx 0.53$ as compared to a

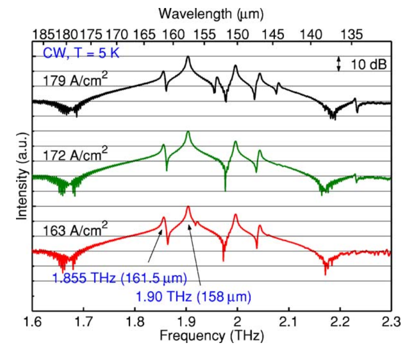

FIG. 2. (Color onlinne) CW spectra on a logarithmic scale measured using a Nicolet 850 spectrometer with a room temperature deuterated triglycine sulfate (DTGS) detector. The spectra were collected using linear scans at a resolution of 0.125 cm^{-1}.

value $\gtrsim 0.8$ in the two-well injector designs[14]). For this reason, a three-well active region design was used to obtain a greater oscillator strength for a given parasitic coupling strength. The downside, however, is that it introduces an upper parasitic level 5 (calculated $E_{54} \sim 15$ meV) that will start sharing a population with level 4 as the electrons become hot, thus reducing gain at higher temperatures. In theory, designs with more than three wells in the active region could provide even greater oscillator strengths but these designs introduce even more undesirable states that are potential sources of parasitic current channels.

The structure, labeled OWI185-M1 (growth EA1304), was grown in GaAs/$Al_{0.15}Ga_{0.85}As$ by molecular beam epitaxy with 185 cascaded modules, with $n = 5 \times 10^{18}$ cm^{-3} contact layers grown above (50 nm thick) and below (100 nm thick) the 10 μm thick active region, and with a 200 nm $Al_{0.55}Ga_{0.45}As$ etch-stop layer underlying the entire growth. The structure was fabricated into a double-metal waveguide since it offers near unity mode confinement and lower losses at low frequencies (surface losses in the metal are $\propto \sqrt{\omega}$). The fabrication was done using copper-to-copper thermocompression wafer bonding, back side substrate removal, and dry etching to form the ridges as described in Ref. 14. The final thickness of the n^+ GaAs receptor substrate in the fabricated devices was lapped down to 140 μm. The fabricated devices were cleaved (with back-facets left uncoated), indium soldered ridge side up on a copper mount, wire bonded, and mounted on the cold stage in a vacuum cryostat. Lasing down to 1.855 THz ($\lambda = 161.5$ μm) was observed from a 97 μm wide and 1.05 mm long ridge device. Figure 2 shows cw spectra taken from this device at 5 K measured at different bias conditions.

Figures 3(a) and 3(b) show the measured optical power versus current (*L-I*) characteristics for the same device. In pulsed operation, the device lased up to a maximum heatsink temperature ($T_{\max}$) of 110 K. The threshold current density (J_{th}) at 5 K was 142 A/cm^2. A fit of J_{th} to the empirical relation $J_{\mathrm{th}} = J_0 + J_1 \exp(T/T_0)$ yields $T_0 = 30$K, a value smaller than that of the higher frequency QCL designs with two-well injectors.[14] This is unexpected, since lower frequency terahertz QCLs are expected to have more robust temperature performance (due to a larger energy barrier $\hbar\omega_{LO} - \hbar\omega_{\mathrm{rad}}$ for thermally activated LO-phonon scattering). This behavior, however, is attributed to the aforementioned upper parasitic level 5 that possibly reduces gain at higher temperatures. Quantitatively, the energy barrier of this thermal back filling process is $E_{54} \sim 15$ meV, as compared to

Downloaded 24 Mar 2006 to 18.62.10.37. Redistribution subject to AIP license or copyright, see http://apl.aip.org/apl/copyright.jsp

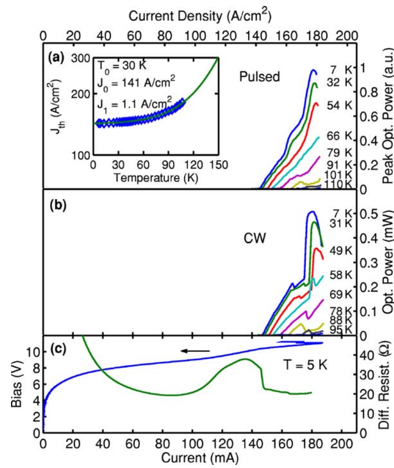

FIG. 3. (Color online) (a) Pulsed and (b) cw *L-I* characteristics measured using a room-temperature pyroelectric detector (Molectron, model P4-42). In pulsed operation the device was biased with pulse trains of 200 ns pulses repeated at 100 kHz, modulated by a 1 kHz square wave with an effective duty cycle of 1%. The inset of panel (a) shows a fit of pulsed J_{th} to the empirical relation $J_{th}=J_0+J_1\exp(T/T_0)$. (c) CW *V-I* and dV/dI-*I* characteristics at a heat sink temperature of 5 K.

that of $\hbar\omega_{LO}-\hbar\omega_{rad}\approx 24$ meV in Ref. 14. Nevertheless, it is interesting to note that $k_B T_{max}/\hbar\omega\approx 1.2$ in this laser, the highest such value for any solid state laser. In cw operation, this device lased up to T_{max}=95K. At 5 K, J_{th} was 143 A/cm^2, and ~0.5 mW of peak cw power was detected from a single facet when collected with a Winston cone (with a circular opening of 1.90 mm diameter) and measured with a thermopile detector (ScienTech, model AC2500) placed adjacent to the cryostat window. At 5 K the single-facet slope efficiency was ~14.5 mW/A (~1.8 photons/electron/facet) without correcting for power lost from the device to the detector. Figure 3(c) shows the cw voltage versus current (*V* -*I*) and differential resistance versus current (dV/dI-*I*) plots measured at 5 K. The lasing threshold is characterized by a kink in the *V-I* that is due to a discontinuous drop in differential resistance at onset of lasing.[10] The relative size of this discontinuity $\Delta R/R$ is a measure of the ratio of upper level and lower level lifetimes. At 5 K, $\Delta R/R$ in this device was 0.32, which is about half of the value for a 3.0 THz laser designed with two-well injectors.[14] This is possibly due to the smaller collector anticrossing gap in this design as was previously discussed. The trough in the differential resistance before threshold indicates lowering of resistance to the current flow at parasitic bias. The device lases beyond the parasitic bias when injector level 1′ starts injecting carriers into the upper level 4.

It is difficult to accurately determine the waveguide losses (α_w) in this structure. The smallest of the cavities tested (including a 97 μm diameter cylindrical disk that supports only $\epsilon_r A/\lambda_0^2\approx 4$ modes) lased with similar threshold current densities. Due to sub-wavelength dimensions of the waveguide aperture, the mirror losses (α_m) in the ridge waveguides are expected to be low.[15] A finite-element simulation for an infinite-width waveguide yielded α_m ~1.3 cm^{-1} for a 1 mm long cavity due to emission from both facets, corresponding to a mirror reflectivity of ~88%. For a finite-width structure, α_m will be even smaller.[15] Devices with lengths of ~0.5 mm, 1 mm, and 2 mm and the same width were tested and all had a J_{th} of ~140 A/cm^2 at 5 K. This could be explained by the fact that J_{th} at 5 K is mostly limited by the parasitic current channel ($1'\rightarrow 2$) and is not a good measure of the losses in the structure. However, the longer devices in general had more cw power output. This result could be used to estimate an upper bound on α_w due to free-carrier losses in the structure. Assuming constant threshold and peak current densities, the peak power output from a ridge laser of length L is $\propto 1/(\alpha_w+\alpha_m)$, where $\alpha_m \propto 1/L$. The increase of cw power in going from 0.5 mm length to a length of 1 mm was typically 50%–100%, whereas further increase in the length had diminishing gains. These observations suggest that α_w is on the order of α_m ~1 cm^{-1} in this structure. A Drude model calculation yielded surface losses of 4–5 cm^{-1} in the metal, and $\lesssim$0.5 cm^{-1} in the thin doped contact layers at top and bottom. This indicates that losses due to the active region itself are small in this structure, which is our main motivation to pursue the one-well injector design.

It is quite encouraging to note that, even though the free-carrier absorption loss scales as λ^2, the lasing threshold current density J_{th} at this long wavelength is still as low as ~140 A/cm^2, which is lower than all the published results of resonant-LO-phonon THz QCLs. In fact, the insensitive dependence of J_{th} on the cavity length strongly indicates that it is the parasitic current, rather than the free-carrier absorption loss, that determines J_{th}. Our investigation suggests that the free-carrier absorption loss, at least in the one-well injector QCL structures described in this letter, will not prevent lasing at even longer wavelength. The main challenge is to design suitable QCL structures that minimize the parasitic current channel while preserving large peak current densities.

The authors would like to thank Hans Callebaut for helpful discussions. This work is supported by AFOSR, NASA, and NSF. Sandia is a multiprogram laboratory operated by Sandia Corporation, a Lockheed Martin Company, for the United States Department of Energy under Contract No. DE-AC04-94AL85000.

[1]J. Faist, F. Capasso, C. Sirtori, D. L. Sivco, A. L. Hutchinson, S. N. G. Chu, and A. Y. Cho, Electron. Lett. **29**, 2230 (1993).
[2]J. Faist, F. Capasso, D. L. Sivco, C. Sirtori, A. L. Hutchinson, and A. Y. Cho, Science **264**, 553 (1994).
[3]R. Köhler, A. Tredicucci, F. Beltram, H. E. Beere, E. H. Linfield, A. G. Davies, D. A. Ritchie, R. C. Iotti, and F. Rossi, Nature (London) **417**, 156 (2002).
[4]G. Scalari, L. Ajili, J. Faist, H. Beere, E. Linfield, D. Ritchie, and G. Davies, Appl. Phys. Lett. **82**, 3165 (2003).
[5]B. S. Williams, S. Kumar, Q. Hu, and J. L. Reno, Electron. Lett. **40**, 431 (2004).
[6]C. Worral, J. Alton, M. Houghton, S. Barbieri, H. E. Beere, D. Ritchie, and C. Sirtori, Opt. Express **14**, 171 (2006).
[7]G. Scalari, S. Blaser, J. Faist, H. Beere, E. Linfield, D. Ritchie, and G. Davies, Phys. Rev. Lett. **93**, 237403 (2004).
[8]B. S. Williams, H. Callebaut, S. Kumar, Q. Hu, and J. L. Reno, Appl. Phys. Lett. **82**, 1015 (2003).
[9]Q. Hu, B. S. Williams, S. Kumar, H. Callebaut, S. Kohen, and J. L. Reno, Semicond. Sci. Technol. **20**, S228 (2005).
[10]C. Sirtori, F. Capasso, J. Faist, A. L. Hutchinson, D. L. Sivco, and A. Y. Cho, IEEE J. Quantum Electron. **34**, 1722 (1998).
[11]H. Callebaut and Q. Hu, J. Appl. Phys. **98**, 104505 (2005).
[12]M. C. Wanke, F. Capasso, C. Gmachl, A. Tredicucci, D. L. Sivco, A. L. Hutchinson, S. N. G. Chu, and A. Y. Cho, Appl. Phys. Lett. **78**, 3950 (2001).
[13]A. Friedrich, G. Boehm, M. C. Amann, and G. Scarpa, Appl. Phys. Lett. **86**, 161114 (2005).
[14]B. S. Williams, S. Kumar, Q. Hu, and J. L. Reno, Opt. Express **13**, 3331 (2005).
[15]S. Kohen, B. S. Williams, and Q. Hu, J. Appl. Phys. **97**, 053106 (2005).

Downloaded 24 Mar 2006 to 18.62.10.37. Redistribution subject to AIP license or copyright, see http://apl.aip.org/apl/copyright.jsp